JOURNAL OF GEOPHYSICAL RESEARCH, VOL. 114, B04406, doi:10.1029/2008JB005763, 2009

Progressive strain localization in a major strike-slip fault exhumed from midseismogenic depths: Structural observations from the Salzach-Ennstal-Mariazell-Puchberg fault system, Austria

Erik Frost,[1] James Dolan,[1] Charles Sammis,[1] Brad Hacker,[2]
Joshua Cole,[2] and Lothar Ratschbacher[3]

Received 23 April 2008; revised 12 September 2008; accepted 22 January 2009; published 15 April 2009.

[1] Analysis of a strike-slip fault exhumed from midseismogenic depths reveals that the fault experienced progressive strain localization toward a high-strain fault core. We focus on the Ennstal segment of the 400-km-long Salzach-Ennstal-Mariazell-Puchberg (SEMP) strike-slip fault system in the Eastern Alps, which accommodated ~60 km of left lateral displacement during Oligo-Miocene time. Macroscopic and microscopic observations reveal a zoned fault featuring a high-strain core at least 10 m wide within a fault zone that is at least 150 m wide. Grain-size distribution analysis shows how the Ennstal segment of the SEMP evolved. Our data reveal a 10-m-wide high-strain fault core (characterized by a power law relationship of grain sizes, $D_2 \approx 2.0$) bordered by a 54-m-wide "transition zone" where the largest and smallest grains are characterized by two power law relationships ($D_2 \approx 2.0$ and 1.6, respectively). This zone is in turn bordered by a region with grain sizes that show a single low-strain power law relationship of $D_2 \approx 1.6$. We interpret these relationships to be the result of concentrated shear overprinting an initial low-strain, power law grain-size distribution before strain localized to the core. This is consistent with the theory that faults mature by smoothing geometrical complexities, forming a highly localized, high-strain fault core. The data do not support the idea that damage forms primarily in response to dynamic stresses during seismic rupture, although they do suggest that this mechanism may operate within tens of meters of the fault once it has developed its zoned structure.

Citation: Frost, E., J. Dolan, C. Sammis, B. Hacker, J. Cole, and L. Ratschbacher (2009), Progressive strain localization in a major strike-slip fault exhumed from midseismogenic depths: Structural observations from the Salzach-Ennstal-Mariazell-Puchberg fault system, Austria, *J. Geophys. Res.*, *114*, B04406, doi:10.1029/2008JB005763.

1. Introduction

[2] One of the most important frontiers in earthquake science is the linkage between the structure and mechanical behavior of fault zones. In particular, little is known about how fault zone structure varies as a function of depth, from near the surface down through the seismogenic crust and into the ductile lower crust. Studies of exhumed faults have delineated the presence in many outcrops of a meters-thick core that has accommodated the bulk of fault displacement, often localized into several centimeters to some decimeters of ultracataclasite [*Anderson et al.*, 1983; *Chester and Chester*, 1998; *Chester et al.*, 1993; *Chester and Logan*, 1986; *Caine et al.*, 1996; *Evans et al.*, 2000; *Faulkner et al.*, 2003; *Wibberley and Shimamoto*, 2003]. The fault core may exhibit strong foliation, as well as distinct, millimeters-thick planar structures that are interpreted to have served as principal slip surfaces. This area is bordered by a gouge and breccia zone that is generally noncohesive, coarser grained, and lacks the shear structures characteristic of the fault core. The verge of the fault zone is marked by fractured wall rock, where fracture density gradually decreases away from the fault to the regional background level.

[3] The actual process by which this zoned fault structure develops remains unresolved. Quasi-static models suggest that zoning occurs in structurally mature, large-displacement faults in which initial geometrical complexity has been reduced, at scales ranging from millimeters to kilometers. *Power et al.* [1987], for example, proposed that fractal surface roughness on a fault would lead to the development of a high-strain fault core that widens with increasing displacement, as larger and larger asperities are eliminated. This idea can be extended to the scale of step overs, as the discontinuities between small faults are eliminated to create a smooth, throughgoing fault plane [*Segall and Pollard*, 1983; *Wesnousky*, 1988]. In quasi-static models, the gouge and breccia zone outside the fault core is viewed as a relict feature

[1]Department of Earth Sciences, University of Southern California, Los Angeles, California, USA.
[2]Department of Earth Science, University of California, Santa Barbara, Santa Barbara, California, USA.
[3]Geowissenschaften, Technische Universität Bergakadamie Freiberg, Freiberg, Germany.

0148-0227/09/2008JB005763$09.00

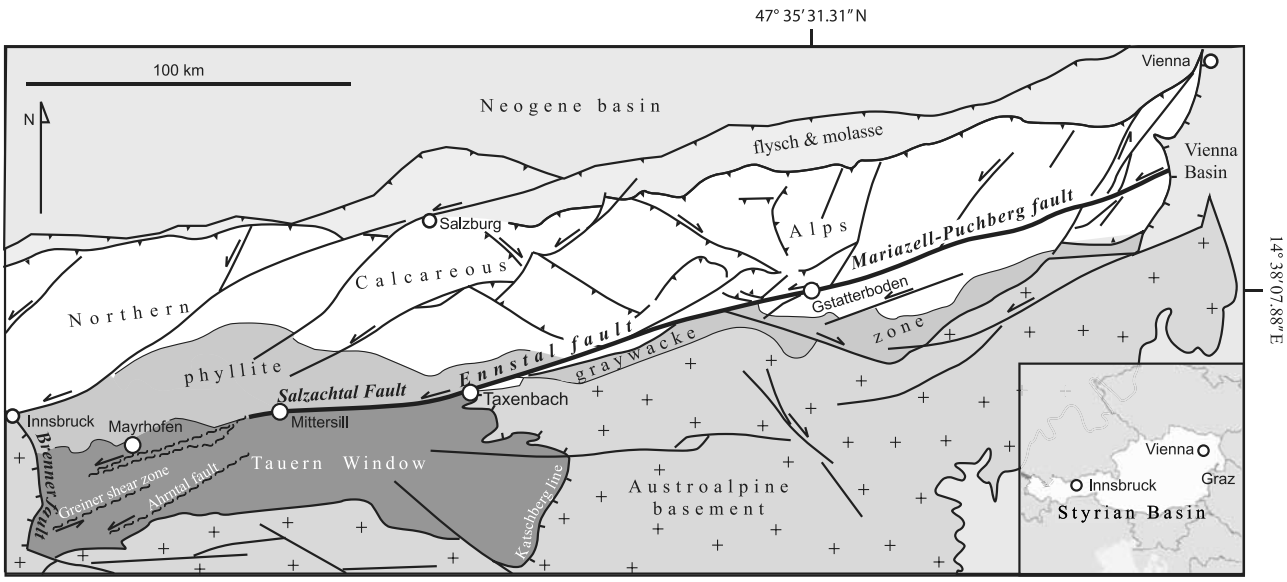

Figure 1. The Salzach-Enntal-Mariazell-Puchberg fault zone and major structural features of the Eastern Alps (after *Linzer et al.* [2002] and *Cole et al.* [2007]). Differential exhumation of the fault exposes a range of exhumation depths along strike from ductile shear zones in the Tauern Window to brittle-ductile outcrops near Taxenbach and finally brittle fault zones of decreasing exhumation depth to the east. Our study site just north of Gstatterboden is at the eastern end of the Ennstal fault segment, exposing the upper seismogenic crust. A detailed geologic map of the Gstatterboden study area is shown in Figure 2.

that accommodated shear strain early in the fault's history, before strain localized to a narrow fault core.

[4] An alternative hypothesis is that fault core gouge forms dynamically during seismic ruptures [*Rice et al.*, 2005]. In this model, stress concentrated at the tip of each passing earthquake rupture cracks and shears the rocks near (within ~40 m) the rupture plane. Each subsequent earthquake reworks the gouge, resulting in a zoned fault. In this model, the fault core is again understood to be a high-strain feature, but the gouged and brecciated rocks outside the core are thought to have shattered in place by seismic waves and experienced only minimal strain.

[5] These hypotheses are not mutually exclusive, and in fact may operate simultaneously. Both predict the presence of a high-strain fault core, with perhaps a greater width expected in the dynamic model. Outside the fault core, the quasi-static model predicts that the gouge and breccia zone has experienced more shear strain than in the dynamic model. In order to better understand the relative contribution of each process to the evolution of a fault zone, it is therefore necessary to examine how strain is distributed throughout the entire fault zone, and whether the mechanics of fragmentation are the same inside and outside the fault core.

[6] In this study, we examine the strain gradient and fragmentation mechanisms at an outcrop of the Salzach-Ennstal-Mariazell-Puchberg (SEMP) fault system, a 400-km-long strike-slip fault system with ~60 km of displacement in the Eastern Alps that has been differentially exhumed such that it exposes a continuum of structural levels along strike, from the near-surface downward across the seismic zone, through the brittle-ductile transition, and into the ductile lower crust. The results of this study allow us to assess the factors governing fault evolution in the brittle upper crust, and, combined with future studies at deeper outcrops, provide a comprehensive picture of the mechanical behavior of a major fault zone.

2. Geologic Overview

[7] The Salzach-Ennstal-Mariazell-Puchberg fault is a primarily sinistral strike-slip fault zone that extends 400 km across the Eastern Alps (Figure 1) [*Ratschbacher et al.*, 1991a, 1991b; *Linzer et al.*, 2002]. From west to east, the Salzach fault forms the northern boundary of the Tauern window (exposing European (Penninic) units beneath African (Austroalpine) units), the Ennstal fault forms the boundary between the central part of the Northern Calcareous Alps and the basement of the Austroalpine unit, and the Mariazell-Puchberg fault cuts the southern margin of the eastern part of the Northern Calcareous Alps. The Northern Calcareous Alps constitute the Late Permian to Cretaceous cover sequence of the Austroalpine basement unit and consist of mostly massive limestone and dolomite and interbedded shale and evaporite. The Northern Calcareous Alps were transformed into a thin-skinned thrust belt during the Cretaceous and dissected by mostly strike-slip faults during the Oligocene-Recent eastward displacement of crustal wedges in the eastern Alpine-western Carpathian orogen [e.g., *Linzer et al.*, 1995, 2002; *Ratschbacher et al.*, 1991a, 1991b]. Structural and kinematic analysis of the southernmost nappe boundaries of the Northern Calcareous Alps [*Ratschbacher et al.*, 1991a, 1991b; *Decker et al.*, 1994; *Linzer et al.*, 1995] demonstrates that the individual segments of the SEMP constitute a throughgoing fault that accommodated orogen-parallel extension. Models have explained this extension as a result of lateral extrusion [*Ratschbacher et al.*, 1991a, 1991b] or oblique indentation of the South Alpine block [*Rosenberg et al.*, 2004]. Geochronology within the

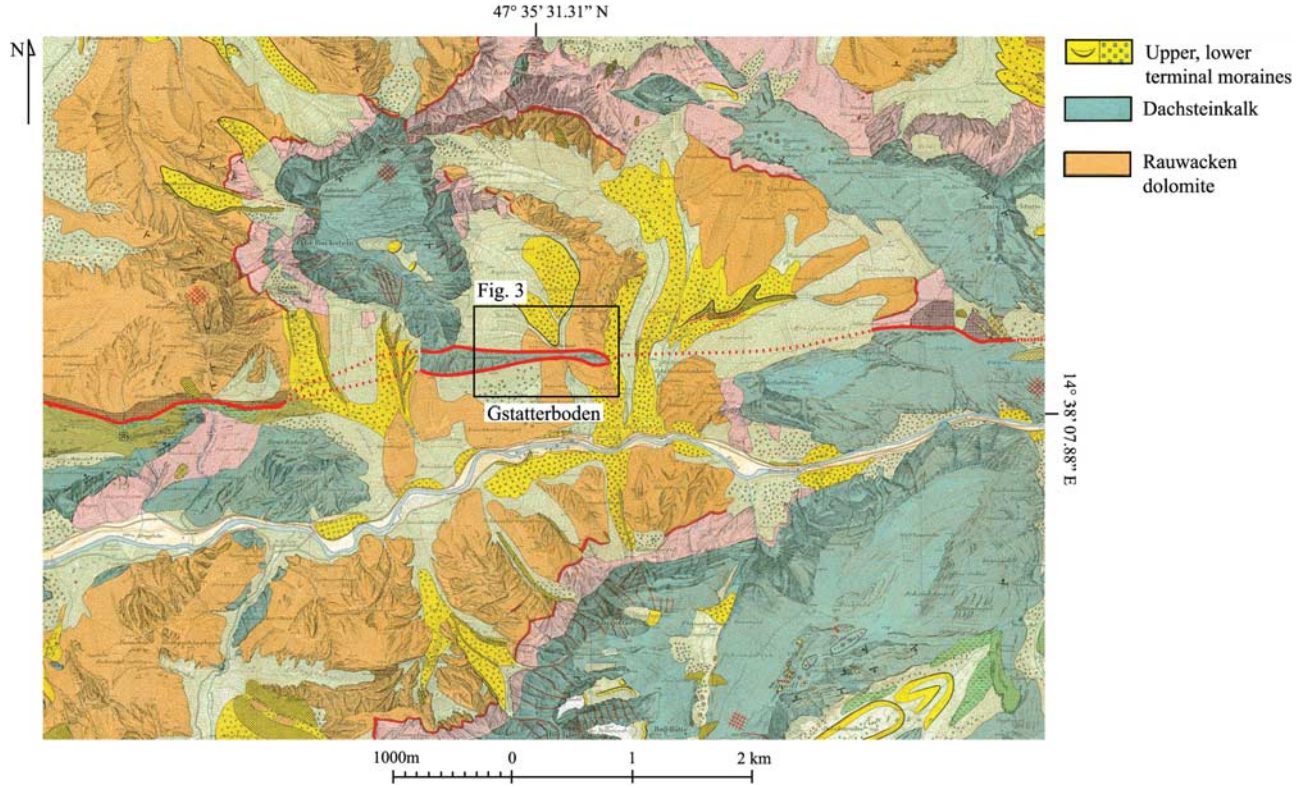

Figure 2. Geologic map of the Gstatterboden study area (from *Ampferer* [1935] with permission from the Austrian Geologische Bundesanstalt). The Ennstal segment of the SEMP has been mapped on the northern and southern boundaries of the Dachsteinkalk sliver. Displacement along the southern fault strand is ~2 km, placing the majority of the ~60 km of fault slip on the northern strand.

Tauern Window and the ages of intraorogenic basins constrain the age of this deformation as Oligocene and Miocene [e.g., *Linzer et al.*, 2002].

[8] The differential exhumation of the SEMP fault zone along strike resulted from greater shortening in the western and central Eastern Alps than in the eastern Eastern Alps, creating an overall higher amount of exhumation in the western part of the Eastern Alps. Combined with subsidence in the easternmost Eastern Alps and Pannonian basin, the entire SEMP fault zone was tilted eastward, resulting in exhumation depths of >20 km in the Tauern Window, decreasing eastward along strike to zero exhumation in the Vienna basin [*Ratschbacher et al.*, 1991a, 1991b]. Deformation structures commensurately change from dominantly ductile where the SEMP enters the Tauern Window at Rinderkarsee [*Cole et al.*, 2007] to ductile-brittle along the eastern end of the Salzachtal segment. Farther east, deformation changes to dominantly brittle along the Ennstal segment before shallowly exhumed levels of the SEMP are revealed along the Mariazell-Puchberg segment.

3. Study Site

[9] The Ennstal segment represents the upper crustal portion of the SEMP (i.e., the "seismogenic zone") along the Northern Calcareous Alps. In this region, the fault also locally branches northward to form NNE-striking thrust faults and duplex structures within the Northern Calcareous Alps; postmiddle Miocene deformation is evident in the SW-directed thrust faults within the sedimentary basins near Wagrain and Hieflau [*Peresson and Decker*, 1997a; *Wang and Neubauer*, 1998]. Total displacement along the Ennstal fault has been estimated at 60 km on the basis of the offset between quartz phyllite units and the Greywacke zone [*Linzer et al.*, 1997, 2002]. Our study site is 1 km north of the town of Gstatterboden at the eastern end of a subtle releasing bend in the Ennstal segment, in the Gesäuse National Park (Figure 1). On the basis of the well-known stratigraphy of the Northern Calcareous Alps, the Rauwacken dolomite at this site should once have been buried by ~4 km of overlying sedimentary rocks [*Geologische Bundesanstalt*, 1980]. However, thrusting across the NCA prior to Miocene strike-slip tectonics [*Linzer et al.*, 1995] is thought to have at least doubled the section. On the basis of these arguments, the Gesäuse outcrop has been exhumed from 4 to 8 km depth.

[10] At the Gesäuse outcrop, the Ennstal fault zone comprises two strands (Figures 2 and 3). The southern strand is poorly exposed along the southern edge of a narrow (100–400 m wide) lens of resistant, cliff-forming limestone of the Dachsteinkalk that appears to have been slivered off a larger body of Dachsteinkalk ~4 km to the east. The northern (main) strand juxtaposes the Dachsteinkalk sliver against Rauwacken dolomite to the north; this strand, which is the focus of this study, has accommodated most of the 60 km of cumulative displacement attributed to this part of the SEMP [*Linzer et al.*, 2002].

[11] At our study site along the northern (main) strand, the fault zone is exposed in a streambed and roadcut. Both

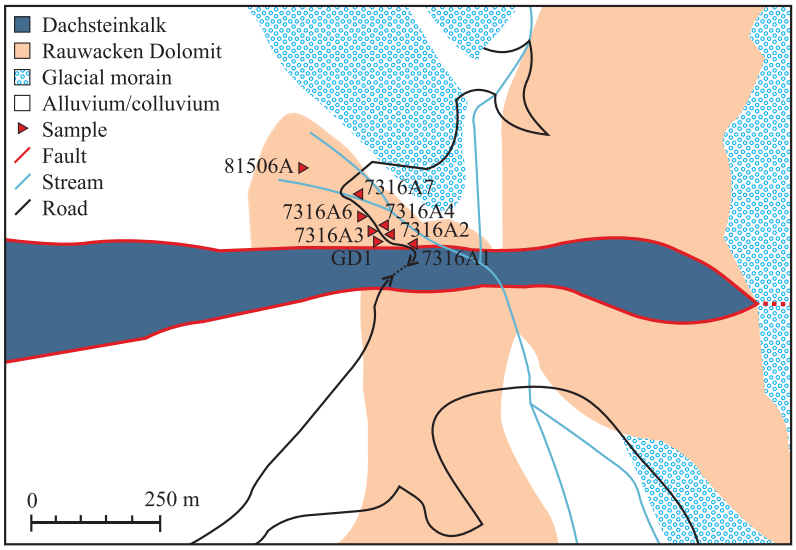

Figure 3. Map of sampling area north of Gstatterboden. Samples of dolomite were collected along the roadcut at 5-m intervals, outcrop permitting, for the first 50 m and then every 50 m beyond that.

exposures provide continuous outcrop of the Rauwacken dolomite for a fault normal distance of ~200 m. Following the stream toward the limestone to the south, however, colluvium and vegetation progressively obscure the outcrop. The Dachsteinkalk unit is better exposed along the roadcut, which provides another 50 m of continuous outcrop south of the fault. Unfortunately, the fault surface at the limestone/dolomite contact along both the road cut and stream exposure is buried beneath a 3–5 m wide section of thick colluvium composed of meter-scale limestone boulders. Notwithstanding the lack of exposure at the fault contact, this study site still allows fundamental observations about the structural evolution of this major strike-slip fault zone.

4. Methods

[12] We documented the major structural properties of this outcrop by measuring the orientation and, where possible, the slip direction and slip sense, of faults and fractures throughout the fault zone. From these measurements, we calculated the reduced stress tensor [*Angelier*, 1984] and associated stress ratio R by the numerical dynamic analysis (NDA) of *Spang* [1972] implemented by *Sperner and Ratschbacher* [1994]. The NDA method assumes an arbitrary shear stress magnitude of 1 acting along each fault in the direction of the striae. Summation of the stress tensors of all fault-striae sets and division by the number of faults yield the bulk stress tensor. The orientation and relative values of the principal stresses are derived from the eigenvalues and eigenvectors of the bulk stress tensor. The stress ratio R, defined as $(\sigma 2 - \sigma 3)/(\sigma 1 - \sigma 3)$, expresses the relationship between the magnitude of the principal stresses. Extreme values of R correspond to stress ellipsoids with $\sigma 2 = \sigma 3$ ($R = 0$; oblate ellipsoid) or $\sigma 1 = \sigma 2$ ($R = 1$; prolate ellipsoid).

[13] We also measured the degree of damage throughout the fault zone at both the macro- and microscales. At the macroscopic scale, the degree of brittle deformation was quantified using damage intensity [*Chester and Logan*, 1986; *Schulz and Evans*, 2000]. Damage elements such as fractures, faults, and shear bands were counted along two perpendicular, 30-cm-long lines at multiple stations along a fault normal transect, and the resulting damage intensities were plotted against perpendicular distance from the fault.

[14] We assessed damage at the microscopic scale by calculating the grain-size distribution of samples taken along the same fault normal transect; the grain-size distribution is considered to indicate the degree of comminution a sample has experienced [*Blenkinsop*, 1991]. Thin sections were cut parallel to the strike of the fault and photographed at magnifications of 25× and 200× with an optical microscope, with the respective photomosaics imaging 4 × 2 cm and 1.9 × 0.9 mm, on average. Areas analyzed at 200× were chosen so as to avoid particles larger than the largest size being counted. Grain sizes were calculated using Image J, an open source image-processing program developed by the National Institutes of Health http://rsb.info.nih.gov/ij/). Gray-scale differences were used to distinguish individual dolomite grains (Figure 4). The grains were then sorted into size classes from 4 mm to 5 μm in diameter, with each class differing from the next by a factor of 2. All graphs are log-log plots of grain size versus grain density, and the power law line of best-fit connecting datapoints is the two-dimensional grain-size distribution, or mass dimension "D_2," of the rock. The standard deviation of each grain-size class is computed by analyzing each image at four threshold values above and below the optimal *Otsu* [1979] threshold (Figure 4).

[15] Calculating the mass dimension of each sample allows us to evaluate proposed fragmentation mechanisms. A number of investigations of natural fault rocks have found that the gouged and brecciated zone outside the fault core produces D_2 values around 1.6 [e.g., *Anderson et al.*, 1983; *Sammis et al.*, 1987; *Chester et al.*, 1993, 2005; *Billi and Storti*, 2004], whereas the fault core rocks are characterized by D_2 values of 2.0 [*Billi and Storti*, 2004; *Chester et al.*, 2005]. These findings are consistent with the "constrained comminution" model for fragmentation [*Sammis et al.*, 1987; *Sammis and King*, 2007]. However, studies of carbonate cataclastic rocks (primarily from the Mattinata fault), have

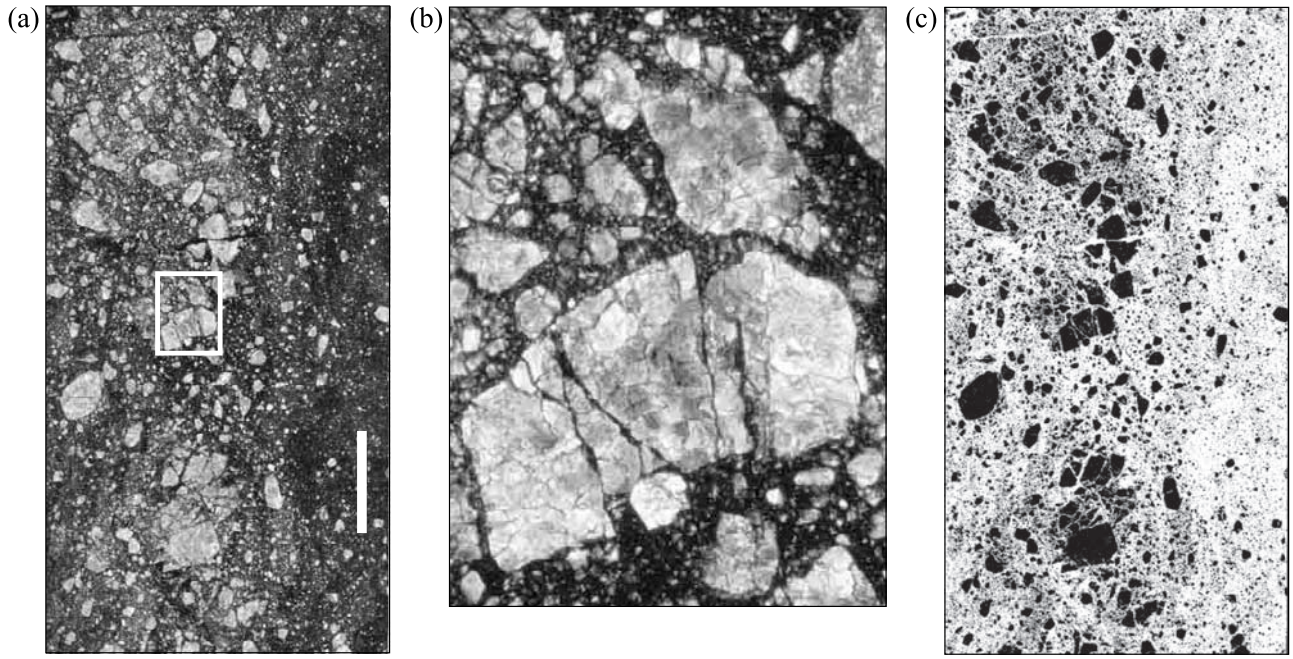

Figure 4. (a) A thin section of dolomite taken ~5 m into our sampling transect, shown at 25× magnification, with a scale bar of 4mm. (b) Magnifying the box highlighted in Figure 4a, we see evidence that grains are composed of distinct smaller particles. This suggests the dolomite may have experienced episodes of fracture and healing, in keeping with predictions from the dynamic model of fault zone evolution. (c) Grains are resolved and analyzed by calculating the optimal gray-scale threshold value via *Otsu*'s [1979] method in Image J. The *Otsu* [1979] threshold is the value that minimizes the gray-scale variance within the foreground and background.

found that D_2 gradually increases from 0.88 at the periphery of the fault zone to 2.5 at the core [*Billi et al.*, 2003; *Billi*, 2007; *Storti et al.*, 2003]. While the basic observation of these papers, that D increases toward localized zones of shear, agrees with findings from other faults zones, the variability of D values reported at carbonate fault zones has led these authors to propose an alternative explanation. *Storti et al.* [2003] suggested that damage in these fault zones is the result of a gradual transition from fragmentation to abrasion as the degree of comminution increases toward the fault core (although it is worth noting that this interpretation does not offer a mechanical explanation of power law grain-size distributions at any D value). It remains unclear whether these differences in mass dimension truly reflect differences in mechanical behavior, or whether they are instead influenced by other factors such as lithology or structural maturity. Our study of cataclastic carbonates from the large-displacement Ennstal segment of the SEMP therefore provides additional insight into the controls governing the mechanics of fragmentation.

5. Results

[16] At the outcrop scale, fault damage along the northern fault strand is asymmetric. South of the fault, the limestone is cut by subsidiary faults and fractures, including meter-scale Riedel shears, but is otherwise largely intact without brecciation (Figure 5). In contrast, the dolomite to the north has been pervasively reduced to millimeter- to centimeter-scale fragments throughout the length of available outcrop (~200-m fault normal distance). The dolomite is also cut by numerous faults and throughgoing fractures, ranging from centimeter-scale fractures with no displacement, to multimeter-long faults with gouge zones up to several centimeters thick. These observations lead us to assume that the fault here was seismogenic because: (1) slow, aseismic fault creep would not generate the brittle features observed in the dolomite and (2) the fault zone at Gstatterboden contains neither evaporite minerals (e.g., salt, gypsum), nor serpentinite, which typically characterize creeping continental faults.

5.1. Structural Data

[17] We measured the orientation, and where possible, the slip direction and slip sense, of >600 faults and fractures in the dolomite along a 160-m-long fault normal transect. When binned in 20-m-wide intervals measured perpendicular to the fault trace, the small-fault data display a distinct pattern (Figures 6). Closest to the limestone-dolomite fault contact, most of the small faults are subparallel to the master fault and subvertical. For the intervals between 20 and 100 m, the dominant small fault set is conjugate to the master fault with N and NNE strikes and dips that shallow farther from the main fault. Beyond 100 m, subsidiary fault orientations appear to be more evenly distributed, with little evidence for a preferred fault set.

[18] These data show that, at least within the first 100 m of the master fault, subsidiary faults occur in two key orientations. The fault-parallel orientation is most clearly expressed within the 20 m closest to the master fault, and diminishes

Figure 5. (a) The Dachsteinkalk to the south of the Ennstal fault is cut by subsidiary faults and fractures but does not show any evidence of brecciation; (b) the Rauwacken dolomite to the north (compare to Figure 5a). (c and d) The dolomite is pervasively shattered and sheared throughout the width of available outcrop (~200 m), presenting what appears at first glance to be a very consistent degree of damage throughout the outcrop.

with distance as the N and NNE conjugate fault orientation becomes more dominant. This transition coincides with the increasing activity of normal and thrust faulting with distance to the master fault, also reflected in the general increase in the stress ratio R (Figure 6). A more detailed kinematic analysis of the small fault data is unwarranted because outcrop conditions greatly limited our ability to measure lineations (and therefore constrain R).

[19] We interpret this pattern to indicate the presence of a high-strain fault core within the 20 m closest to the master fault, possibly extending out as far as ~40 m. Small faults in this interval are almost exclusively fault parallel, with dips noticeably steeper than in any other interval. This is consistent with observations from other exhumed fault cores, which tend to exhibit fault-parallel foliations and shear structures [e.g., *Chester et al.*, 1993; *Schulz and Evans*, 2000].

5.2. Relative Strain Distribution

[20] To further estimate the fault-perpendicular strain gradient within the fault zone, we quantified both macro- and microscopic damage. Calculation of the macroscopic damage intensity taken along a fault-perpendicular transect clearly reflects the asymmetric damage pattern, with almost all the deformation accommodated in the dolomite (Figure 7). Within the dolomite, damage intensity is greatest close to the fault and decreases by ~25% at a distance of 150 m. These results could be due to a very high background level of deformation within the dolomite, which would blur the distinction between fractured wall rocks outside the fault zone and damage within the gouge and breccia zone, or could instead reflect the fact that at this depth, the brittle fault zone is at least 150 m wide. To determine whether our results are complicated by high levels of background deformation, we also examined microscopic grain-size distributions from samples along the same fault-perpendicular transect (Figure 3). Samples that are characterized by a power law relationship of grain sizes would indicate the activity of one of several mechanical processes thought to be active within the fault core and gouge and breccia zones. The lack of a power law relationship, however, would suggest that the given sample is outside the fault zone, in the fractured wall rocks. In other words, the presence of a power law distribution would indicate the creation of damage elements through fault-related shear strain, whereas the absence of a power law distribution would imply comminution without significant shear strain (e.g., in situ shattering near the lithologic contact, or unrelated background deformation at the margin of the fault zone).

[21] Samples of dolomite closest to the fault (within the 10 m of dolomite adjacent to the covered interval) yielded mass dimensions of $D_2 \approx 2.0$ (Figures 8 and 9). At a distance of 109 m from the fault, the mass dimension of the dolomite has fallen to a value of $D_2 \approx 1.6$. Between these samples, however, the distribution of grain sizes is best characterized by two power law relationships. For samples

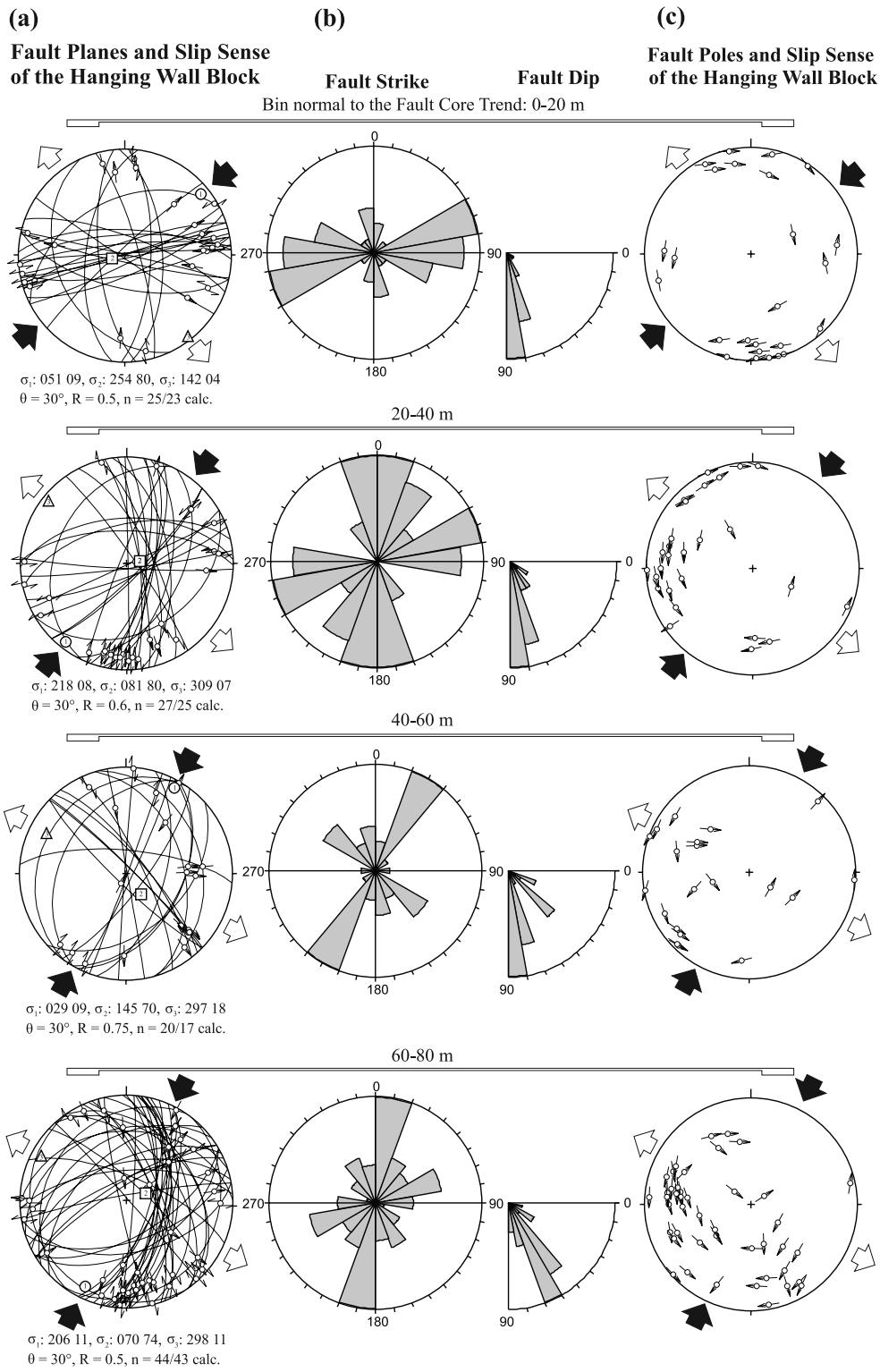

Figure 6. (a) Lower hemisphere, equal area fault-striae diagrams for each 20-m fault trend normal bin with reduced stress tensor. Parameters shown are $\sigma 1 \geq \sigma 2 \geq \sigma 3$, the principal stresses; θ, the dihedral angle between $\sigma 1$ and the fault measured in the plane that contains the pole to the fault and the associated striae; R, the stress ratio; n, the number of fault-striae measurements plotted; n-calc, the number of measurements used for calculation. Faults are drawn as great circles and striae are drawn as arrows pointing in the direction of hanging wall transport. Arrows around the plots give calculated local orientation of subhorizontal principal compression and extension. (b) Histogram of fault strike in 20° azimuth intervals and fault dip in 10° intervals for each 20-m bin. (c) As the great circle diagrams in Figure 6a get illegible with large data sets, the fault-striae data of Figure 6a are also plotted as poles to fault planes and with corresponding lineations drawn in the pole points as tangents to the common great circle of the fault pole and lineation.

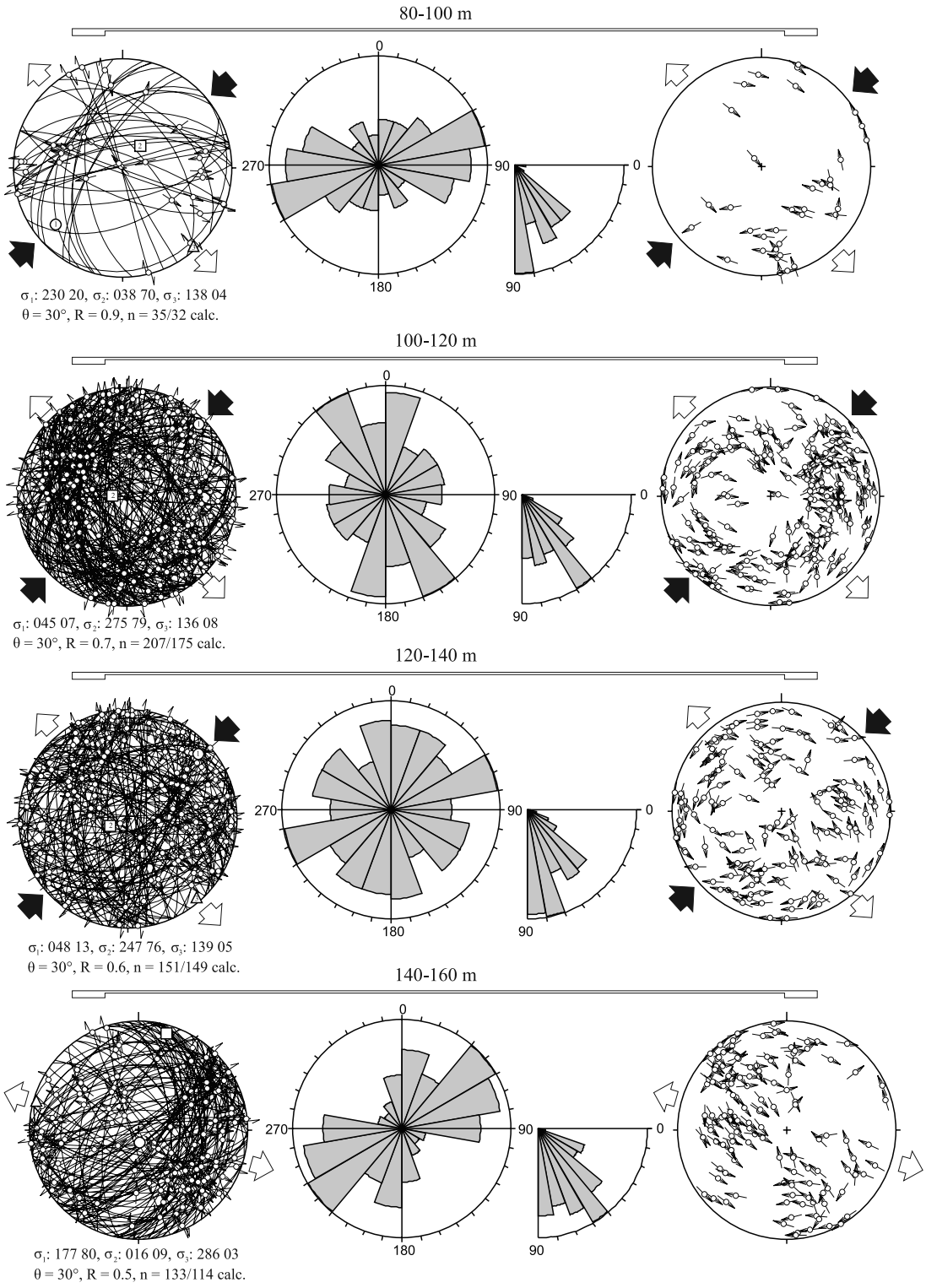

Figure 6. (continued)

taken 10 m to 64 m from the fault, the mass dimension at 25× magnification is ~2.0, whereas the mass dimension at 200× magnification is always closer to 1.6 (Figure 9). The largest grains, in effect, share the characteristics of a high-strain gouge typically found near shear localizations, whereas the smallest grains more closely resemble what is typically found in a gouge and breccia zone. Such a pattern has not been reported from any other exhumed fault as far as we are aware.

6. Discussion

[22] These observations of fault zone structure can be used to evaluate the evolutionary processes that shaped the

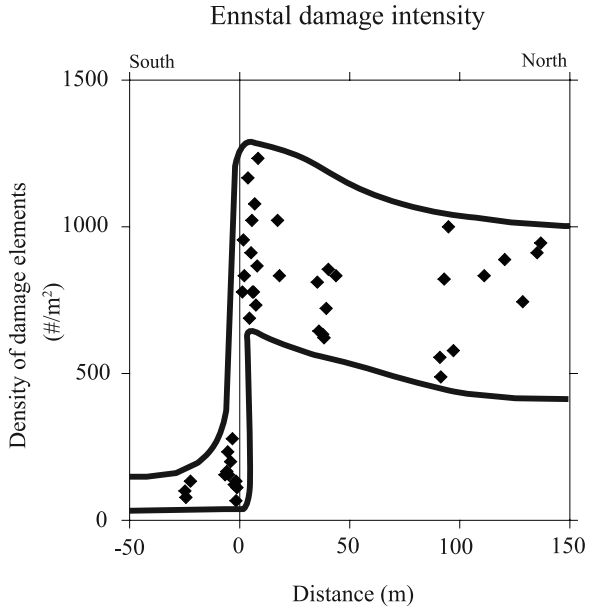

Figure 7. Measurements of macroscopic damage intensity along the Ennstal segment of the SEMP at Gstatterboden clearly reflect the asymmetric damage pattern observed between the limestone and dolomite. Damage intensity decreases by ~25% at a distance of 150 m in the dolomite. This could reflect either a very high background level of damage, or a fault zone that has distributed strain throughout at least 150 m during its lifetime.

Ennstal fault. End-member models of fault zone evolution propose that the zoned structure commonly found in exhumed faults is created by either dynamic or quasi-static stresses. The dynamic model predicts that each earthquake rupture cracks and shears the rocks close to (within ~40 m) the rupture plane, while the gouge and breccia zone rocks are shattered in place and experience almost no strain [*Rice et al.*, 2005]. Quasi-static models, on the other hand, require the entire width of the fault zone to experience strain as increasing displacement eliminates geometrical complexities, bringing larger and larger asperities into contact.

[23] Although we do not observe a clear structural zonation at the outcrop scale such as a fault core characterized by ultracataclasites and principal slip surfaces bordered by a less cohesive zone of gouge and breccia, our measurements of small-fault data and grain-size distributions indicate a clear zonation of strain. The presence of numerous fault-parallel, subvertical subsidiary strike-slip faults in the 20–40 m of dolomite closest to the fault contact suggests that displacement was preferentially accommodated in this region. Furthermore, samples taken within 10 m of the fault contact display mass dimensions of $D_2 \approx 2.0$ at all grain sizes, a feature unique to high-strain fault cores [*Billi et al.*, 2003; *Chester et al.*, 2005]. These data indicate that the fault core at this outcrop of the Ennstal fault is at least 10 m wide, possibly extending out to 40 m. The decrease in mass dimensions beyond 10 m, first seen in the smallest grains and eventually in all grains, combined with an increase in the variability of subsidiary fault orientations beyond 40 m, suggests that the fault core is bordered by a zone of lower-strain brecciation. Additionally, the bimodal distribution of power law grain-size distributions observed out to a distance of 109 m is consistent with the fragmentation mechanism of constrained comminution operating throughout the dolomite [*Sammis et al.*, 1987; *Sammis and King*, 2007], indicating that the relatively strong damage intensity observed as far as 100–150 m from the fault contact represents deformation within the fault zone. This is perhaps not surprising, given that other studies of carbonate fault zones document widths of 200–300 m [e.g., *Billi et al.*, 2003; *Billi and Storti*, 2004].

[24] Our first-order observation of a high-strain fault core surrounded by a low-strain zone of brecciation and gouge is consistent with findings from other exhumed faults that have shown evidence of constrained comminution [*Sammis et al.*, 1987; *Chester et al.*, 1993, 2005; *Evans et al.*, 2000; *Billi and Storti*, 2004]. The fact that we do not find a variety of D values, as reported for carbonates of the Mattinata fault zone [e.g., *Storti et al.*, 2003], leads us to suggest that these differences are not caused by differences in lithology. The major difference between the Mattinata and Ennstal faults is structural maturity: the Mattinata fault is estimated to have accommodated <2 km slip, whereas the Ennstal segment of the SEMP exhibits ~60 km of cumulative displacement [*Linzer et al.*, 2002; *Billi et al.*, 2003]. One effect of lithology, however, may be related to the width of the fault core. In contrast to the Punchbowl and San Gabriel faults, which cut through crystalline and siliciclastic rocks, the high-strain core of the Gstatterboden dolomites, as defined by mass dimensions, is at least an order of magnitude wider. While both quartzofeldspathic and calcite gouges have demonstrated strain-weakening behavior in laboratory experiments [e.g., *Logan et al.*, 1992; *Gu and Wong*, 1994; *Beeler et al.*, 1996], the added presence of mica at the Punchbowl and San Gabriel faults may favor extreme localization. Carbonate fault zones, on the other hand, have been shown to produce fault cores on the order of 20 m wide [*Billi and Storti*, 2004].

[25] Microscopic observations of the Gstatterboden outcrop suggest that this zoned fault structure is the result of progressive localization of strain within the dolomite. As noted above, all samples between 10 and 64 m are characterized by two power laws, with mass dimensions of ~2.0 in the largest grains and ~1.6 in the smallest grains (Figure 9). We propose that this "transition zone" has recorded the history of strain localization within the dolomite during increasing displacement along the SEMP. The development of a gouge with a mass dimension of $D_2 \approx 1.6$ has been demonstrated by experiments to coincide with the transition from velocity strengthening to velocity weakening, which favors strain localization [*Biegel et al.*, 1989]. In contrast, a mass dimension of $D_2 \approx 2.0$ is thought to be the product of concentrated flow shear once strain has localized [*Sammis and King*, 2007]. This second phase of fragmentation reworks the initial, geometrically stable arrangement of grains, placing once isolated grains back into contact with each other, causing one to fracture. Fragmentation starts at the largest grain size because these grains have the highest probability of coming into contact with each other in the low-strain gouge.

[26] Our observations from the transition zone lead us to propose that this zone only partially experienced the second phase of fragmentation as strain localized toward the fault

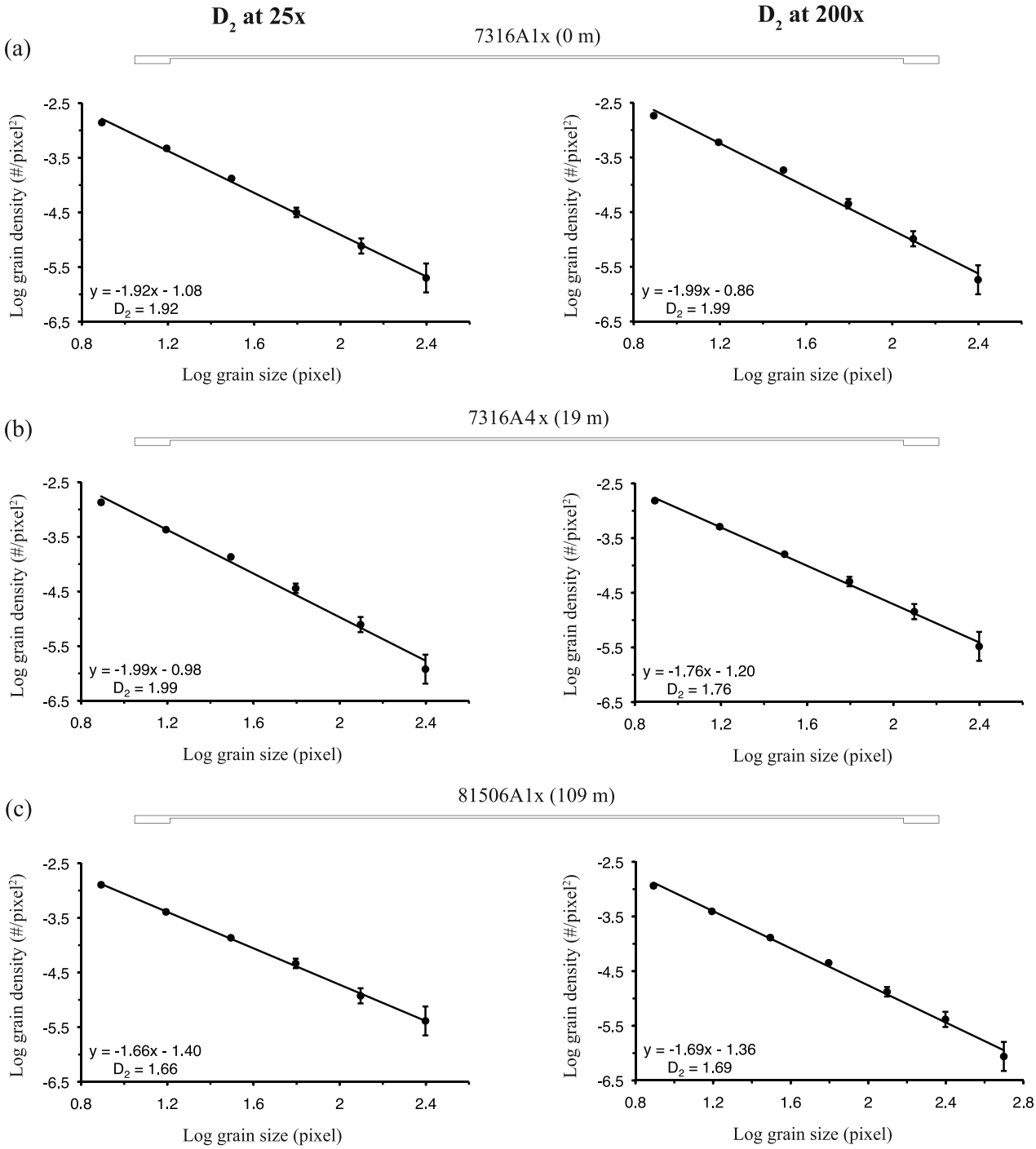

Figure 8. Representative grain-size distribution plots from the three different zones observed. For each sample, grains were sorted into bins on the basis of mean diameter in pixels (534 pixel/mm at 25×, 7 pixel/μm at 200×), with each bin differing from the next by a factor of 2. Grain size was then plotted against relative area fraction for each size bin. (a) Samples within 10 m of the fault display mass dimensions of $D_2 \approx 2.0$ for grains sized 4 mm to 5 μm. (b) Samples 10–64 m from the fault display consistently variable mass dimensions. The largest grains (2 mm to 62.5 μm) produce the typical high-strain fault core mass dimension of $D_2 \approx 2.0$, while the smallest grains (125–5 μm) display more closely resemble damage zone gouge and breccias with a mass dimensions of $D_2 \approx 1.6$. (c) By a distance of 100 m from the fault, mass dimensions are nearer to the typical damage zone value of $D_2 \approx 1.6$ for all grain sizes.

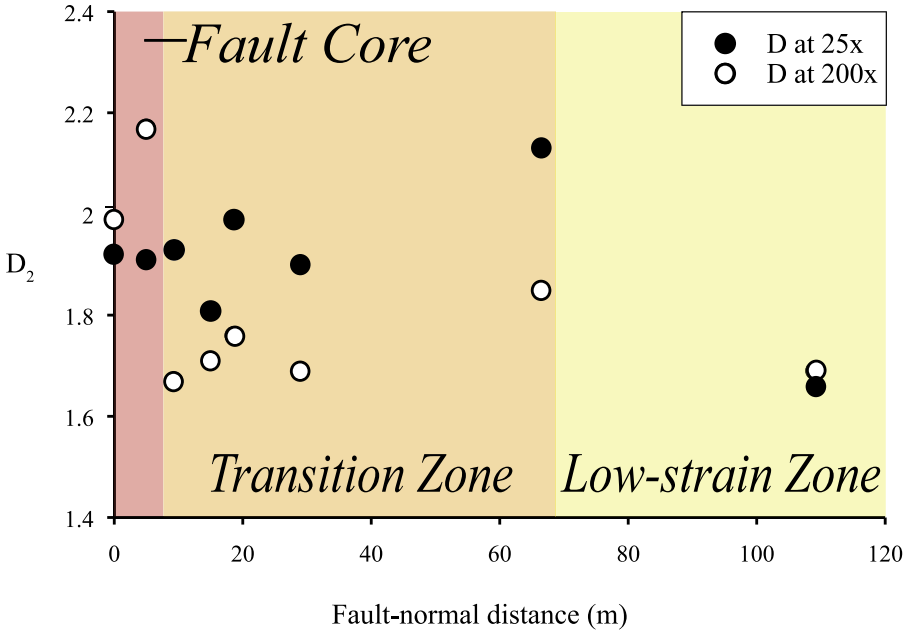

Figure 9. Mass dimensions for the largest (black circles) and smallest (white circles) grains in each sample. Samples closest to the fault produce results typically found in high-strain fault cores. For the five samples from 10 to 64 m in the "transition zone," we find two power law relationships. Understood in the framework of constrained comminution, the largest grains in this zone must have been subject to a high-strain concentrated flow shear, yet the smallest grains show little evidence of this high-strain event. They instead more closely mirror what is seen in a low-strain damage zone.

core. We postulate that the initial phase of localization focused strain into a zone at least 64 m wide (the distance to which a power law relationship of 2.0 can be observed), inducing a concentrated flow shear that reworked the mass dimension of these rocks starting at the largest grain size (Figure 8). Before this second phase of fragmentation could work its way down to the smallest grains, however, strain localized to an even narrower zone, forming the fault core characterized by $D_2 \approx 2.0$ for all grain sizes, and leaving behind a volume of fault rock that records the history of strain localization (Figure 10). We therefore interpret this as a "Type II" fault zone according to the classification of *Means* [1995]. A "Type I" fault, which shows the same strain profile we document here but thickens with time, requires zoning to develop as a result of strain hardening. However, that interpretation is inconsistent with evidence presented here for the activity of constrained comminution. We can think of no mechanical process that would explain a *Means*'s [1995] Type III fault zone, in which strain accumulates in all parts of the fault at the same time, but at a slower rate at the periphery of the fault.

[27] Taken together, these data and interpretations are consistent with the quasi-static model of fault zone evolution, which suggests that our macroscopic observation of pervasively damaged rock at a fault-perpendicular distance of ~150 m from the fault is largely a relic of the early stages of fault formation, reflecting the scale of initial geometrical complexity. However, while our data suggest that quasi-static mechanisms were largely responsible for the formation of the zoned Ennstal fault, it is certainly possible that zoning has been reinforced by dynamic forces. Grains analyzed in thin section are composed of smaller particles that have been cemented together, which could indicate repeated stages of shattering because of dynamic rupture followed by healing (Figure 4).

[28] Our study at Gstatterboden is only one part of a larger investigation of fault zone structure at multiple exhumation depths along the SEMP fault system (Figure 11). By comparing our observations from the seismogenic zone at Gstatterboden with future studies at the brittle-ductile transition, near Taxenbach, and down into the ductile middle crust [*Cole et al.*, 2007; *Rosenberg and Schneider*, 2008], we can reconstruct the three-dimensional structure of the SEMP and evaluate the manner in which the structure of the fault has evolved. Such understanding is vital if we are to understand the mechanical instabilities that control the nucleation and propagation of seismic ruptures.

7. Conclusions

[29] Previous investigations of the structure of exhumed, large-displacement faults have led to the formulation of a zoned fault model in which the majority of slip has been accommodated in a narrow fault core. Whether such zoning is the result of strain localizing toward the fault core during progressive slip along the fault (quasi-static model), dynamic stresses shattering and shearing rocks near the fault plane during successive earthquake ruptures (dynamic model), or a combination of the two, has been a matter of debate. While we find evidence of both processes, we conclude that the Ennstal segment of the SEMP fault zone in Austria evolved primarily by progressive localization of a wide zone of deformation toward a high-strain fault core.

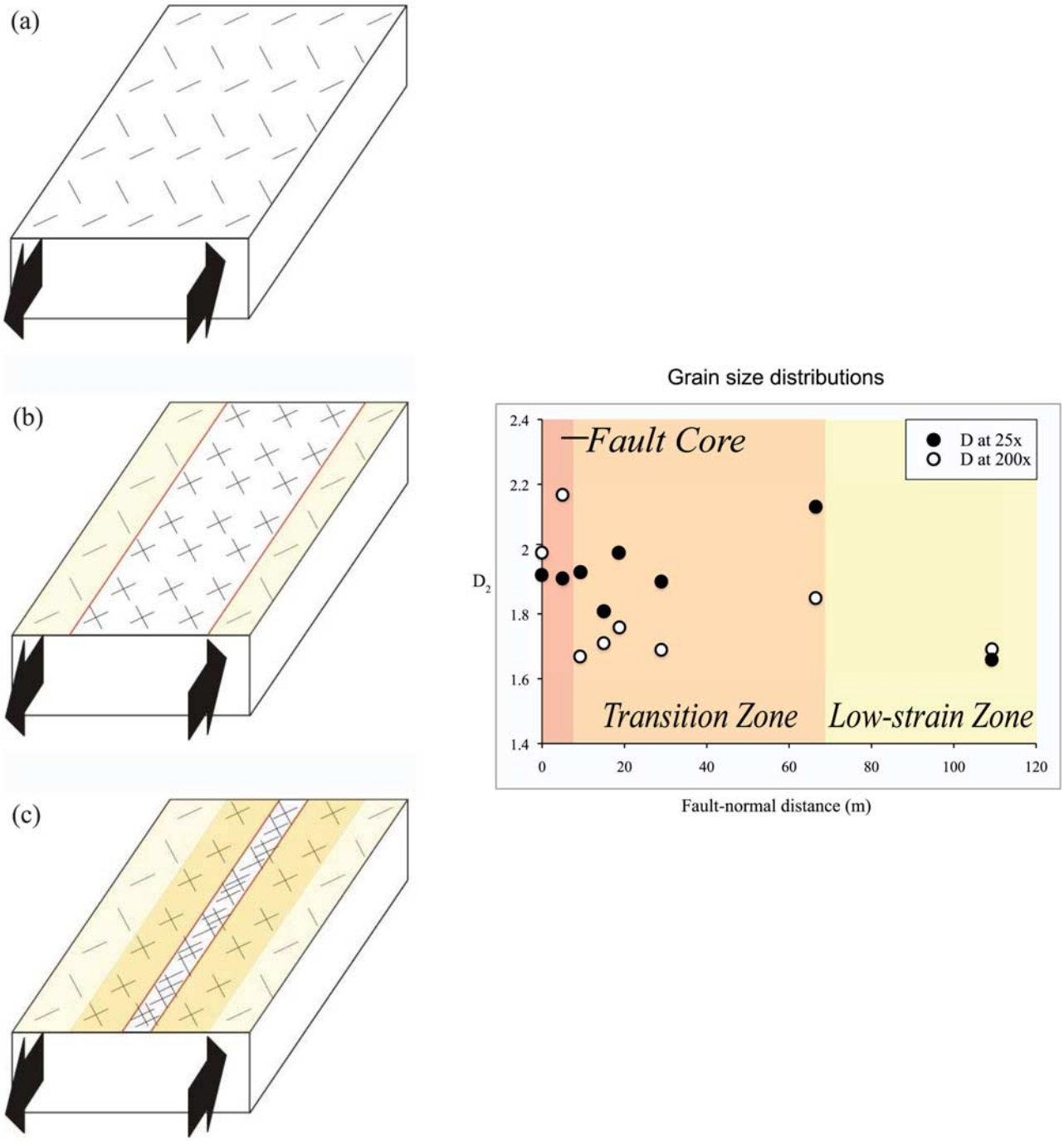

Figure 10. Schematic depiction of strain localization. White regions are the active zones of deformation. (a) During the early stages of fault formation, strain is distributed throughout a wide region. Deformation is accommodated at the grain scale by constrained comminution, which produces a mass dimension of $D_2 \approx 1.6$ everywhere. (b) Since constrained comminution favors shear localization, the next phase of deformation is focused into a narrower region. This concentrated flow shear disturbs the previously stable geometrical arrangement of grains and shifts the mass dimension of the rock toward $D_2 \approx 2.0$, starting at the largest grains. (c) Before the second phase of deformation is completed down to the smallest grains, strain again localizes to what will become the fault core. This leaves behind a volume of rock that records the history of strain localization within the fault zone.

[30] Specifically, grain-size distributions support the idea that the bulk of the slip on the SEMP has been accommodated in a zone at least 10 m wide. Additionally, at least 54 m of dolomite adjacent to the high-strain zone contains structural features typical of both the high-strain core and low-strain gouge and breccia zone. We propose that this transition zone formed as a result of concentrated shear flow that partially overprinted the initial low-strain mass dimension

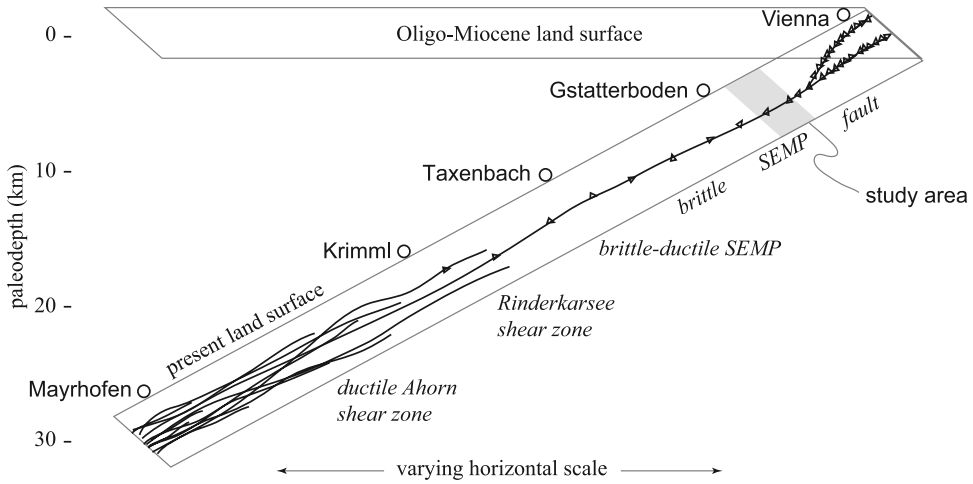

Figure 11. Schematic reconstruction of the SEMP fault system during Oligo-Miocene time (after *Cole et al.* [2007]). At our study site north of Gstatterboden, we observe an asymmetric fault zone at least 150 m wide with a high-strain core ~10 m wide (based on grain-size distributions) and up to 40 m wide (based on small-fault data). At greater exhumation depths (15–25 km), the SEMP is characterized by a series of brittle-ductile and ductile shear zones that span less than 1 km, with the majority of strain accommodated in a single 100-m-wide shear zone [*Cole et al.*, 2007]. At the deepest (>20 km) studied exposures of the SEMP, in the Ahorn shear zone, strain is distributed within a 2-km-wide mylonite belt [*Rosenberg and Schneider*, 2008]. Future work at brittle-ductile exposures of the SEMP near Taxenbach will further constrain the three-dimensional structure of the fault.

in these rocks, creating a record of strain localization along this part of the exhumed SEMP fault system. The possible existence of an even higher-strain fault core within the 3-to-5-m-wide unexposed interval at the fault contact leaves open the possibility that slip in that interval is even more localized. This highlights the fact that evidence for a broad zone of deformation across a fault may only be taken to represent the finite strain that has accumulated over the lifetime of the fault, and that the most recent increment of infinitesimal strain may be confined to a much more discrete zone.

[31] **Acknowledgments.** This research was funded by U. S. National Science Foundation grants EAR-0309542 and EAR-0309995. We thank Kurt Decker (Universität Wien) for sharing his expertise of the SEMP and Ron Biegel (USC) for his insights into grain-size distribution analysis. Jeff Hoeft, Frances Cooper, Edgar Scheidewig, and Veronika Geissler provided invaluable assistance in the field. James Evans and Frederick Chester provided helpful reviews.

References

Ampferer, O. (1935), *Geologische Karte der Gesäuseberge*, Geol. Bundesanst., Vienna.

Anderson, L., R. H. Osbourne, and D. F. Palmer (1983), Cataclastic rocks of the San Gabriel fault: An expression of deformation at deeper crustal levels in the San Andreas fault zones, *Tectonophysics*, *98*, 209–251, doi:10.1016/0040-1951(83)90296-2.

Angelier, J. (1984), Tectonic analysis of fault slip data sets, *J. Geophys. Res.*, *89*, 5835–5848, doi:10.1029/JB089iB07p05835.

Beeler, N. M., T. E. Tullis, M. L. Blanpied, and J. D. Weeks (1996), Frictional behavior of large displacement experimental faults, *J. Geophys. Res.*, *101*, 8697–8715, doi:10.1029/96JB00411.

Biegel, R. L., C. G. Sammis, and J. H. Dieterich (1989), The frictional properties of a simulated gouge having a fractal particle distribution, *J. Struct. Geol.*, *11*, 827–846, doi:10.1016/0191-8141(89)90101-6.

Billi, A. (2007), On the extent of size range and power law scaling for particles of natural carbonate fault cores, *J. Struct. Geol.*, *29*, 1512–1521, doi:10.1016/j.jsg.2007.06.007.

Billi, A., and F. Storti (2004), Fractal distribution of particle size in carbonate cataclastic rocks from the core of a regional strike-slip fault zone, *Tectonophysics*, *384*, 115–128, doi:10.1016/j.tecto.2004.03.015.

Billi, A., F. Salvini, and F. Storti (2003), The damage zone-fault core transition in carbonate rocks: Implications for fault growth, structure and permeability, *J. Struct. Geol.*, *25*, 1779–1794, doi:10.1016/S0191-8141(03)00037-3.

Blenkinsop, T. G. (1991), Cataclasis and processes of particle size reduction, *Pure Appl. Geophys.*, *136*, 59–86, doi:10.1007/BF00878888.

Caine, J. S., J. P. Evans, and C. B. Forster (1996), Fault zone architecture and permeability structure, *Geology*, *24*, 1025–1028, doi:10.1130/0091-7613(1996)024<1025:FZAAPS>2.3.CO;2.

Chester, F. M., and J. S. Chester (1998), Ultracataclasite structure and friction processes of the Punchbowl fault, San Andreas system, California, *Tectonics*, *295*, 199–221.

Chester, F. M., and J. M. Logan (1986), Implications for mechanical properties of brittle faults from observations of the Punchbowl fault zone, California, *Pure Appl. Geophys.*, *124*, 79–106, doi:10.1007/BF00875720.

Chester, F. M., J. P. Evans, and R. L. Biegel (1993), Internal structure and weakening mechanisms of the San Andreas Fault, *J. Geophys. Res.*, *98*, 771–786, doi:10.1029/92JB01866.

Chester, J. S., F. M. Chester, and A. K. Kronenberg (2005), Fracture surface energy of the Punchbowl fault, San Andreas system, California, *Nature*, *437*, 133–136, doi:10.1038/nature03942.

Cole, J., B. Hacker, L. Ratschbacher, J. Dolan, G. Seward, E. Frost, and W. Frank (2007), Localized ductile shear below the seismogenic zone: Structural analysis of an exhumed strike-slip fault, Austrian Alps, *J. Geophys. Res.*, *112*, B12304, doi:10.1029/2007JB004975.

Decker, K., H. Peresson, and P. Faupl (1994), Miocene tectonics in the eastern Limestone Alps; kinematics, paleostress and distribution of deformation during the lateral extrusion of the Central Alps, *Jahrb. Geol. Bundesanst.*, *137*, 5–18.

Evans, J. P., Z. K. Shipton, M. A. Pachell, S. J. Lim, and K. Robeson (2000), The structure and composition of exhumed faults, and their implications for seismic processes, in *Proceedings of the 3rd Conference on Tectonic Problems of the San Andreas Fault System, 6–8 December 2000*, edited by G. Bokelmann and R. L. Kovach, pp. 67–81, Stanford Univ., Palo Alto, Calif.

Faulkner, D. R., A. C. Lewis, and E. H. Rutter (2003), On the internal structure and mechanics of large strike-slip fault zones: Field observations of the Carboneras fault in southeastern Spain, *Tectonophysics*, *367*, 235–251, doi:10.1016/S0040-1951(03)00134-3.

Geologische Bundesanstalt (1980), *Der Geologische Aufbau Österreichs*, 700 pp., Springer, Wien, Germany.

Gu, Y., and T.-F. Wong (1994), Development of shear localization in simulated quartz gouge: Effect of cumulative slip and gouge particle size, *Pure Appl. Geophys.*, *143*, 387–423, doi:10.1007/BF00874336.

Linzer, H. G., L. Ratschbacher, and W. Frisch (1995), Transpressional collision structures in the upper crust of the fold-thrust belt of the Northern Calcareous Alps, *Tectonophysics*, *242*, 41–63, doi:10.1016/0040-1951(94)00152-Y.

Linzer, H. G., F. Moser, R. Nemes, L. Ratschbacher, and B. Sperner (1997), Build-up and dismemberment of a classical fold-and-thrust belt: From non-cylindrical stacking to lateral extrusion in the eastern Northern Calcareous Alps, *Tectonophysics*, *272*, 97–124, doi:10.1016/S0040-1951(96)00254-5.

Linzer, H. G., K. Decker, H. Peresson, R. Dell'Mour, and W. Frisch (2002), Balancing orogenic float of the Eastern Alps, *Tectonophysics*, *354*, 211–237, doi:10.1016/S0040-1951(02)00337-2.

Logan, J. M., C. A. Dengo, N. G. Higgs, and Z. Z. Wang (1992), Fabrics of experimental fault zones: Their development and relationship to mechanical behavior, in *Fault Mechanics and Transport Properties of Rocks*, edited by B. Evans and T.-F. Wong, pp. 33–69, Academic, San Diego, Calif.

Means, W. D. (1995), Shear zones and rock history, *Tectonophysics*, *247*, 157–160, doi:10.1016/0040-1951(95)98214-H.

Otsu, N. (1979), A threshold selection method from gray-level histograms, *IEEE Trans. Syst. Man Cybern.*, *9*, 62–66, doi:10.1109/TSMC.1979.4310076.

Peresson, H., and K. Decker (1997a), Far-field effects of late Miocene subduction in the Eastern Carpathians: E-W compression and inversion of structures in the Alpine-Carpathian-Pannonian region, *Tectonics*, *16*, 38–56, doi:10.1029/96TC02730.

Power, W. L., T. E. Tullis, S. R. Brown, G. N. Boinott, and C. H. Scholz (1987), Roughness of natural fault surfaces, *Geophys. Res. Lett.*, *14*, 29–32, doi:10.1029/GL014i001p00029.

Ratschbacher, L., W. Frisch, H.-G. Linzer, and O. Merle (1991a), Lateral extrusion in the Eastern Alps: 2. Structural analysis, *Tectonics*, *10*, 257–271, doi:10.1029/90TC02623.

Ratschbacher, L., O. Merle, P. Davy, and P. Cobbold (1991b), Lateral extrusion in the Eastern Alps: 1. Boundary conditions and experiments scaled for gravity, *Tectonics*, *10*, 245–256, doi:10.1029/90TC02622.

Rice, J. R., C. G. Sammis, and R. Parsons (2005), Off-axis secondary faulting induced by a dynamic slip-pulse, *Bull. Seismol. Soc. Am.*, *95*, 109–134, doi:10.1785/0120030166.

Rosenberg, C. L., and S. Schneider (2008), The western termination of the SEMP Fault (eastern Alps) and its bearing on the exhumation of the Tauern Window, *Geol. Soc. Spec. Publ.*, *298*, 197–218, doi:10.1144/SP298.10.

Rosenberg, C. L., J. P. Brun, and D. Gapais (2004), Indentation model of the Eastern Alps and the origin of the Tauern Window, *Geology*, *32*, 997–1000, doi:10.1130/G20793.1.

Sammis, C. G., and G. C. P. King (2007), Mechanical origin of power law scaling in fault zone rock, *Geophys. Res. Lett.*, *34*, L04312, doi:10.1029/2006GL028548.

Sammis, C. G., G. C. P. King, and R. Biegel (1987), The kinematics of gouge deformation, *Pure Appl. Geophys.*, *125*, 777–812, doi:10.1007/BF00878033.

Schulz, S. E., and J. P. Evans (2000), Mesoscopic structure of the Punchbowl Fault, southern California and the geologic and geophysical structure of active strike-slip faults, *J. Struct. Geol.*, *22*, 913–930, doi:10.1016/S0191-8141(00)00019-5.

Segall, P., and D. D. Pollard (1983), Nucleation and growth of strike-slip faults in granite, *J. Geophys. Res.*, *88*, 555–568, doi:10.1029/JB088iB01p00555.

Spang, J. H. (1972), Numerical method for dynamic analysis of calcite twin lamellae, *Geol. Soc. Am. Bull.*, *83*, 467–472, doi:10.1130/0016-7606(1972)83[467:NMFDAO]2.0.CO;2.

Sperner, B., and L. Ratschbacher (1994), A Turbo Pascal program package for graphical presentation and stress analysis of calcite deformation, *Z. Dtsch. Geol. Ges.*, *145*, 414–423.

Storti, F., A. Billi, and F. Salvini (2003), Particle size distributions in natural carbonate fault rocks: Insights for non-self-similar cataclasis, *Earth Planet. Sci. Lett.*, *206*, 173–186, doi:10.1016/S0012-821X(02)01077-4.

Wang, X., and F. Neubauer (1998), Orogen-parallel strike-slip faults bordering metamorphic core complexes: The Salzach-Enns fault zone in the Eastern Alps, Austria, *J. Struct. Geol.*, *20*, 799–818, doi:10.1016/S0191-8141(98)00013-3.

Wesnousky, S. G. (1988), Seismological and structural evolution of strike-slip faults, *Nature*, *335*, 340–342, doi:10.1038/335340a0.

Wibberley, C. A. J., and T. Shimamoto (2003), Internal structure and permeability of major strike-slip fault zones: The Median Tectonic Line in Mie Prefecture, southwest Japan, *J. Struct. Geol.*, *25*, 59–78, doi:10.1016/S0191-8141(02)00014-7.

J. Cole and B. Hacker, Department of Earth Science, University of California, Santa Barbara, Webb Hall, Building 526, Santa Barbara, CA 93106-9630, USA.

J. Dolan, E. Frost, and C. Sammis, Department of Earth Sciences, University of Southern California, 3651 Trousdale Parkway, Los Angeles, CA 90089, USA. (efrost@usc.edu)

L. Ratschbacher, Geowissenschaften, Technische Universität Bergakademie Freiberg, D-09599 Freiberg, Germany.